Synthesis and Characterization of Near Infrared Cu-In-Se/ZnS Core/Shell Quantum Dots For *in vivo* Imaging

E. Cassette,[†] *T. Pons,*[†,*] *C. Bouet,*[†] *M. Helle,*[‡] *L. Bolotine,*[‡] *F. Marchal,*[‡] *B. Dubertret*[†]

[†] Laboratoire de Physique et Etude des Matériaux, UMR8213, ESPCI, CNRS, Université Pierre et Marie Curie, 10, rue Vauquelin, 75005 Paris, France, and [‡] Centre de Recherche en Automatique de Nancy, Nancy-University, CNRS, Centre Alexis Vautrin, avenue de Bourgogne, 54511 Vandoeuvre-lès-Nancy Cedex, France

Supplementary information

Cu-In-Se HRTEM pictures

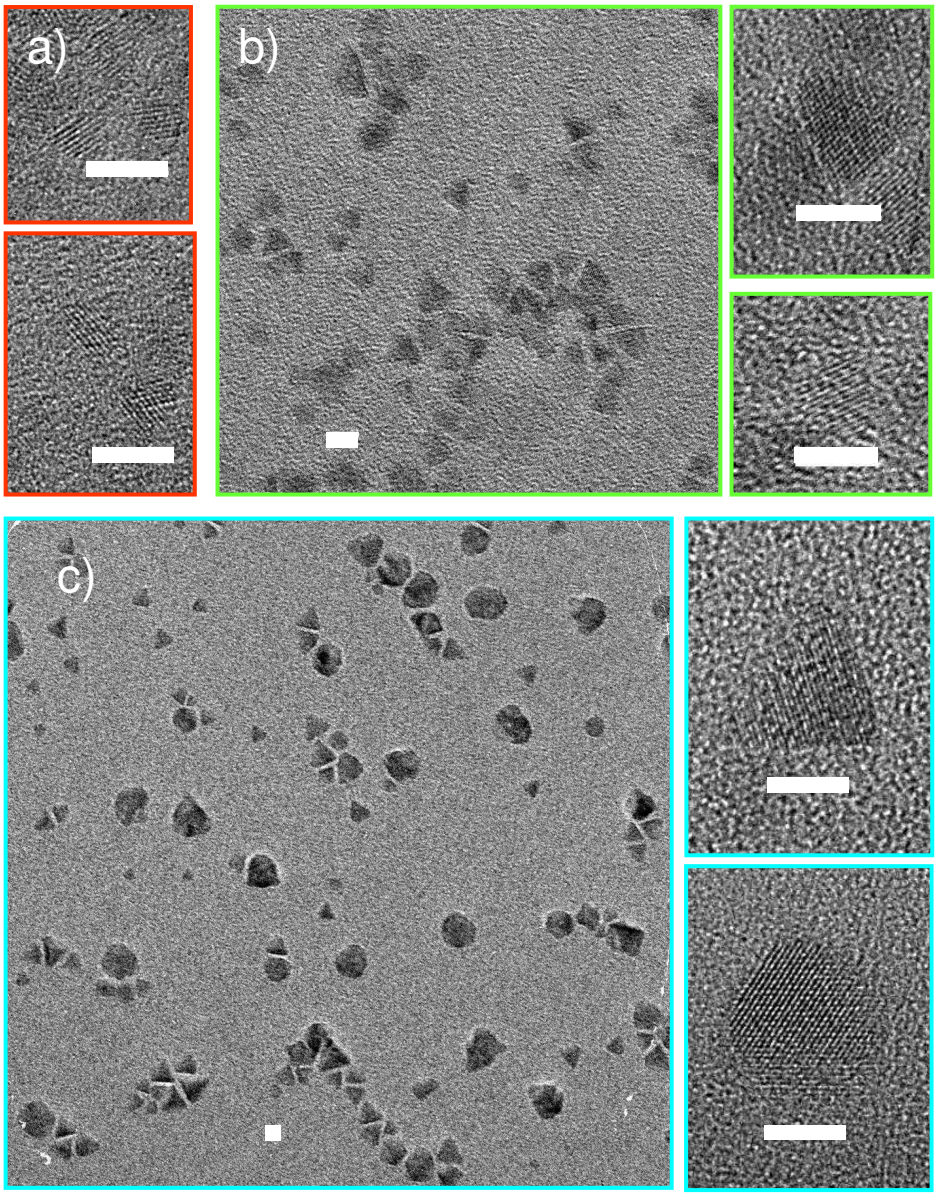

Figure S1: HRTEM pictures of Cu-In-Se core QDs synthesized a) at 180 °C (3.0 ± 0.6 nm in diameter), b) 250 °C-intermediate reaction (5.0 ± 1.1 nm) and c) 250 °C-slow reaction (8.3 ± 1.9 nm). Scale bar: 5 nm.

Comparison of TEM and XRD size estimations

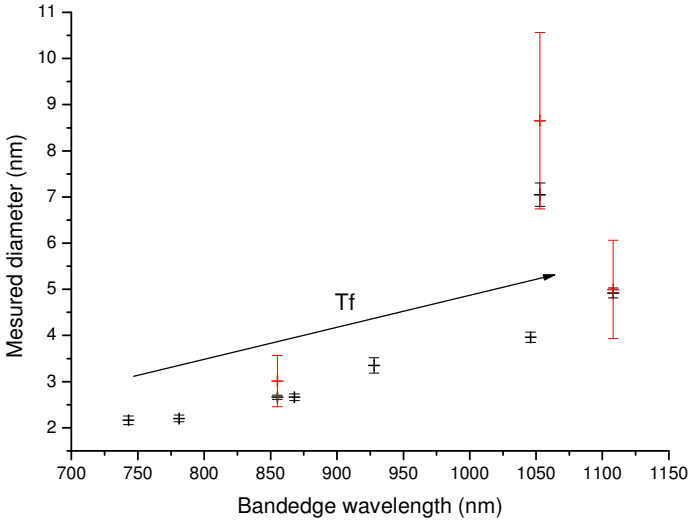

Figure S2: Cu-In-Se QD sizes estimated by XRD (black) are plotted versus the effective bandgap determined by absorption spectra (see below) and compared to TEM measurements (red). All samples were synthesized by fast heating except the samples about 5 and 8 nm which were synthesized at 250 °C with an intermediate and a 1h heating rise respectively.

Bandgap determination:

The first absorption peak was not well defined, which may due to the size and the composition dispersion of the QD samples. As a consequence we chose to attribute the effective bandgap to the position of the intersection between the $y = 0$ line and the tangent at the inflection point of the red shoulder (Fig. S3).

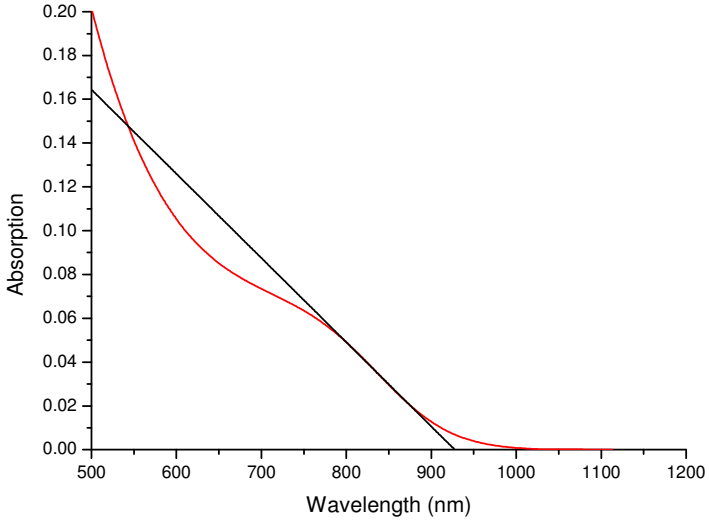

Figure S3: Example of the effective bandgap determination. In red, the absorption spectrum of the sample synthesized at 220 °C with fast heating and in black the tangent at the inflection point. Here the effective bandgap was attributed to 1.34 eV which corresponds to wavelength of 928 nm.

QD composition measured by EDX

T_f (°C)	In/Cu	Cu/Se	In/Se	S/Se
140	2.04 ± 0.18	0.30 ± 0.04	0.62 ± 0.03	0.35 ± 0.01
160	1.71 ± 0.07	0.39 ± 0.02	0.66 ± 0.02	0.25 ± 0.003
180	1.54 ± 0.01	0.43 ± 0.03	0.66 ± 0.03	0.22 ± 0.01
200	1.35 ± 0.05	0.48 ± 0.03	0.65 ± 0.02	0.26 ± 0.01
220	1.25 ± 0.13	0.52 ± 0.07	0.65 ± 0.04	0.18 ± 0.03
250	1.14 ± 0.02	0.60 ± 0.03	0.68 ± 0.03	0.28 ± 0.01

Table ST1: QD composition ratios measured by EDX for each sample synthesized by fast heating to the indicated T_f. The S proportion was mostly attributed to the DDT around the NCs.

Estimation of the composition of the QD volume deposited during the growth:

During the fast heating synthesis, the temperature rises constantly, and the QDs progressively grow as the temperature increases. For each reaction temperature T_f, we call V_f the volume of the particle, $N_{f,A}$ (A = Cu, In, Se) the number of atoms A in the QD and $C_{f,A}$ their concentration. ΔV_f and $\Delta N_{f,A}$ refer to the difference in volume and number of atoms A between the sample at temperature *f* and the first sample (T_1 = 140 °C):

$$\Delta V_f = V_f - V_1$$
$$\Delta N_{f,A} = N_{f,A} - N_{1,A}$$
$$N_{f,A} = C_{f,A} * V_f$$

We then use the sizes measured by DRX to estimate V_f and the composition ratios measured by EDX $(Cu/Se)_f$ and $(In/Se)_f$, which are proportional to $C_{f,Cu}/C_{f,Se}$ and $C_{f,In}/C_{f,Se}$ respectively:

$$N_{f,Cu} = V_f * (Cu/Se)_f * C_{f,Se}$$

We further assume that that the defects in the QDs are primarily due to Cu and In vacancies and substitutions, so that the concentration of Se in the QD is constant. We then obtain

$$\Delta N_{f,A} \propto V_f * (Cu/Se)_f - V_1 * (Cu/Se)_1.$$

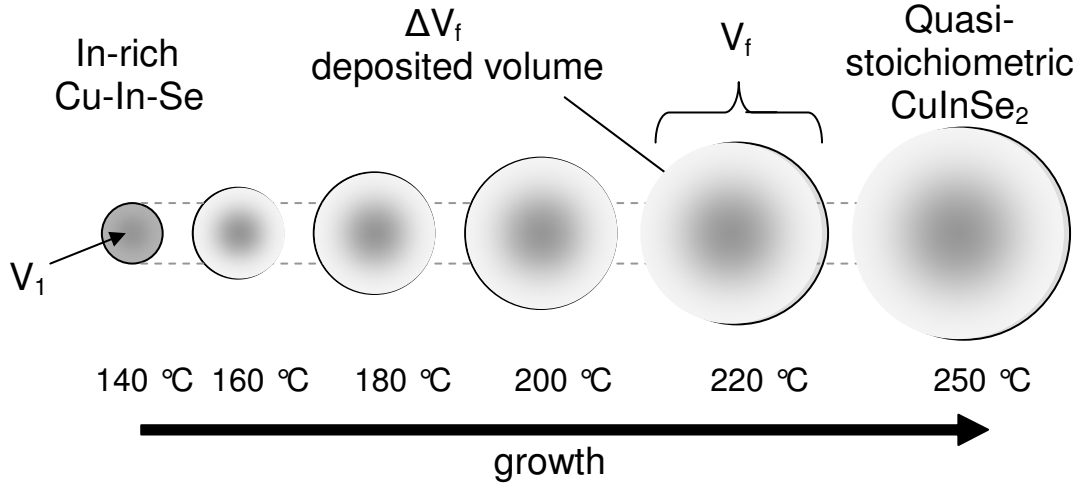

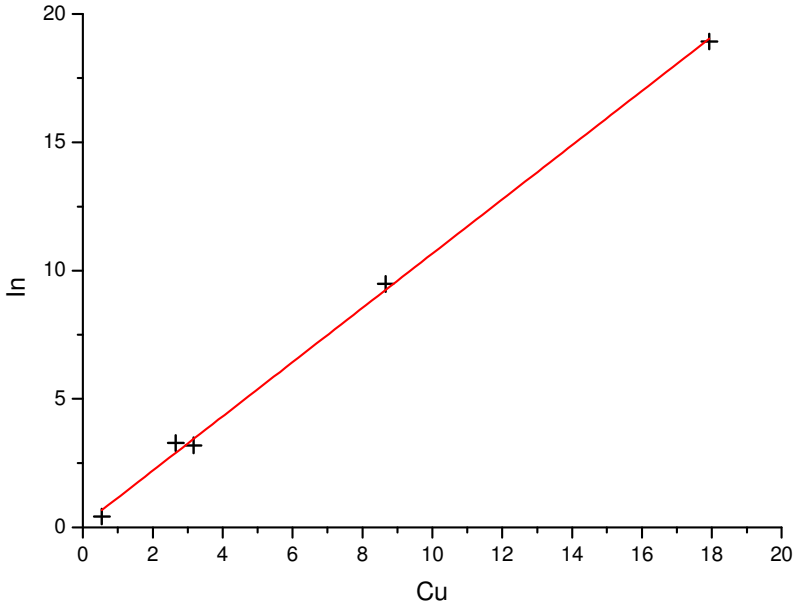

Figure S4: Indium and copper proportions in the volume deposited between T = 140 °C and subsequent growth temperatures. The line corresponds to a linear fit (slope of 0.94 ± 0.02).

Room temperature fluorescence decay of Cu-In-Se core and Cu-In-Se core/shell QDs

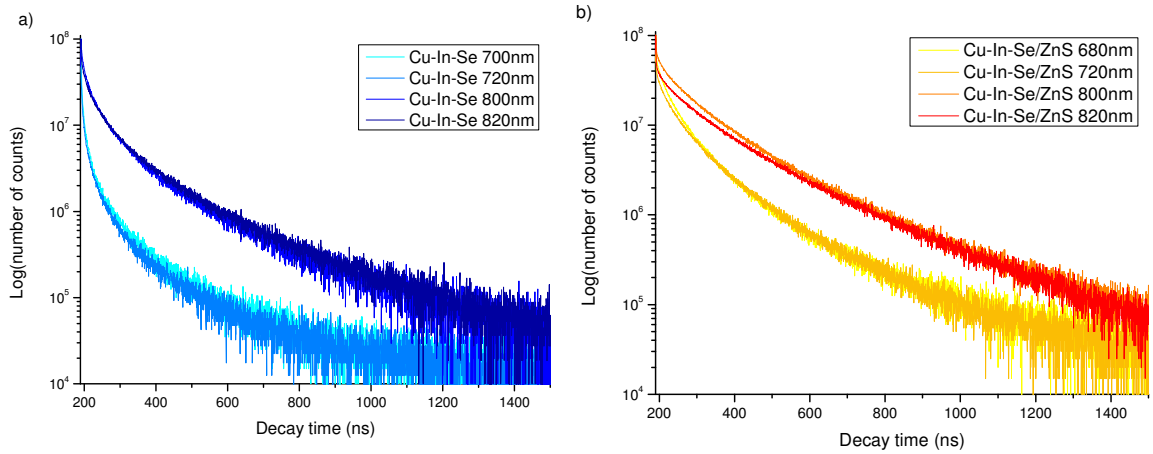

Figure S5: Room temperature fluorescence decay of a) Cu-In-Se core and b) Cu-In-Se/ZnS core/shell QDs for different emission wavelengths. All measurements show an important long life time (170-275ns). We noted that the proportions of long decay time increased with the emission wavelength, which is consistent with recombination via donor-acceptor levels located in the bandgap.

Evolution of the PL and the absorption band gap energy

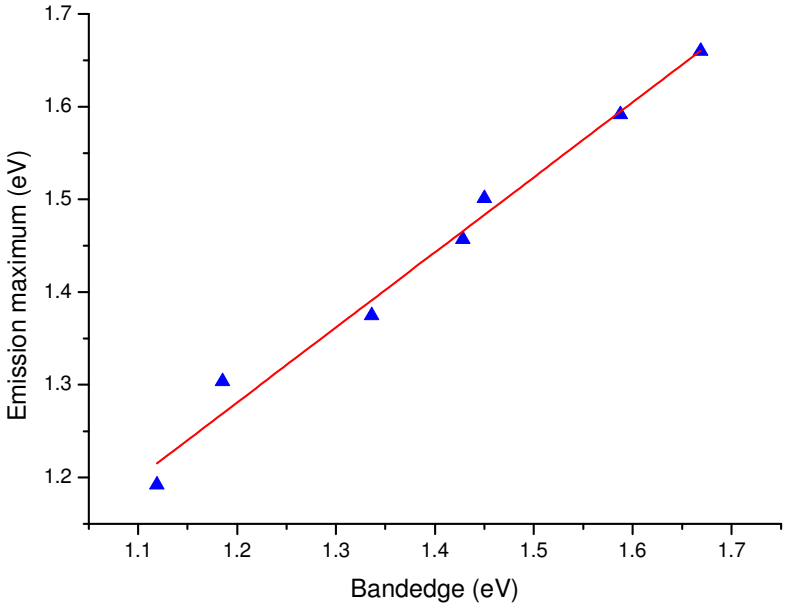

Figure S6: The PL maximum energy is plotted versus the effective bandgap. The line corresponds to a linear fit with a slope of 0.81 ± 0.04.

Size distributions

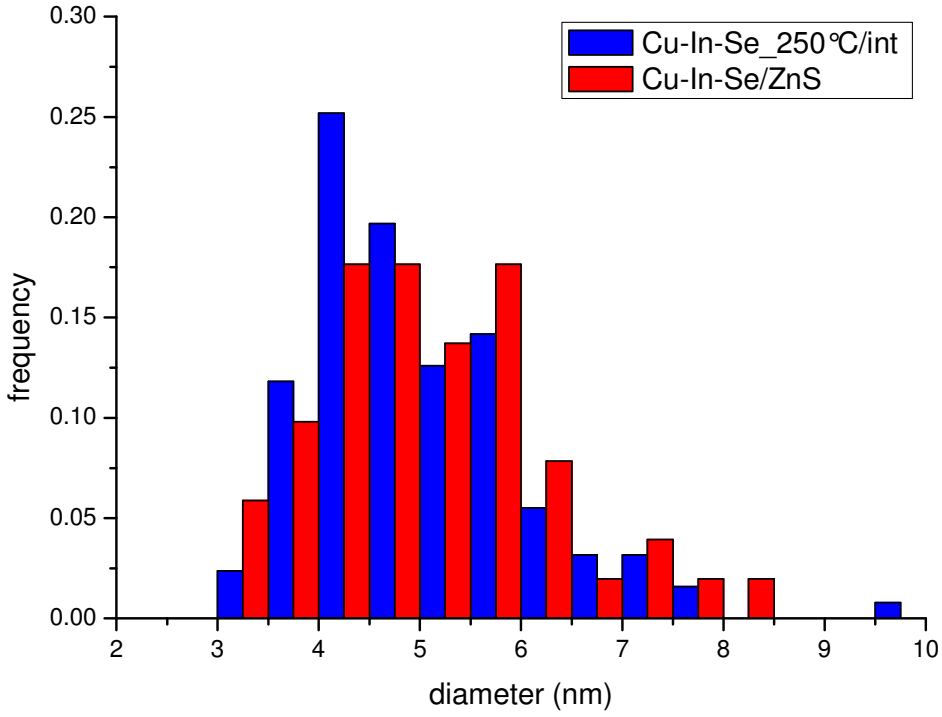

Figure S7: TEM size distribution of $CuInSe_2$ and $CuInSe_2$/ZnS QDs. The core sample was synthesized at 250 °C with an intermediate heating. The average particle size is 5±1.1 nm for $CuInSe_2$ and 5.1±1.1 nm for the corresponding $CuInSe_2$/ZnS.

***In vivo* imaging.**

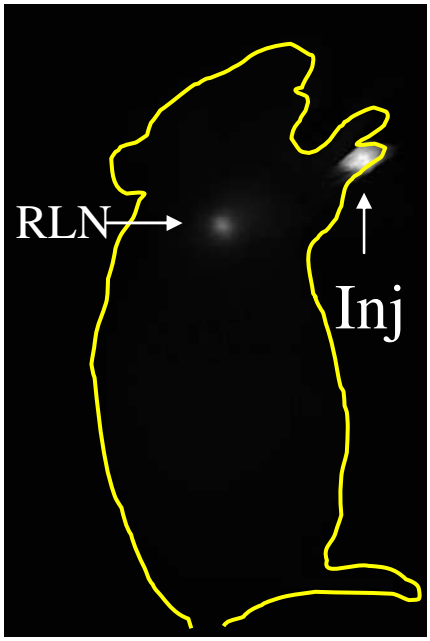

Figure S8: *In vivo* imaging of the right flank of the mouse at 4h post injection, showing the injection point (Inj) and the regional lymph node (RLN).